



# Exploring the severe winter haze in Beijing: the impact of synoptic weather, regional transport and heterogeneous reactions

G. J. Zheng<sup>1</sup>, F. K. Duan<sup>1</sup>, H. Su<sup>2</sup>, Y. L. Ma<sup>1</sup>, Y. Cheng<sup>1</sup>, B. Zheng<sup>1</sup>, Q. Zhang<sup>3,6</sup>, T. Huang<sup>4</sup>, T. Kimoto<sup>4</sup>, D. Chang<sup>2</sup>, U. Pöschl<sup>2</sup>, Y. F. Cheng<sup>2</sup>, and K. B. He<sup>1,5,6</sup>

<sup>1</sup>State Key Joint Laboratory of Environment Simulation and Pollution Control, School of Environment, Tsinghua University, Beijing 100084, China

<sup>2</sup>Multiphase Chemistry Department, Max Planck Institute for Chemistry, 55128, Mainz, Germany

<sup>3</sup>Ministry of Education Key Laboratory for Earth System Modeling, Center for Earth System Science, Tsinghua University, Beijing 100084, China

<sup>4</sup>Kimoto Electric Co., Ltd, 3-1 Funahashi-cho Tennoji-ku, Osaka 543-0024, Japan

<sup>5</sup>State Environmental Protection Key Laboratory of Sources and Control of Air Pollution Complex, Beijing 100084, China

<sup>6</sup>Collaborative Innovation Center for Regional Environmental Quality, Beijing 100084, China

Correspondence to: K. B. He (hekb@mail.tsinghua.edu.cn) and Y. F. Cheng (yafang.cheng@mpic.de)

Received: 16 April 2014 – Published in Atmos. Chem. Phys. Discuss.: 3 July 2014

Revised: 6 January 2015 – Accepted: 14 January 2015 – Published: 17 March 2015

**Abstract.** Extreme haze episodes repeatedly shrouded Beijing during the winter of 2012–2013, causing major environmental and health problems. To better understand these extreme events, we performed a model-assisted analysis of the hourly observation data of PM<sub>2.5</sub> and its major chemical compositions. The synthetic analysis shows that (1) the severe winter haze was driven by stable synoptic meteorological conditions over northeastern China, and not by an abrupt increase in anthropogenic emissions. (2) Secondary species, including organics, sulfate, nitrate, and ammonium, were the major constituents of PM<sub>2.5</sub> during this period. (3) Due to the dimming effect of high loading of aerosol particles, gaseous oxidant concentrations decreased significantly, suggesting a reduced production of secondary aerosols through gas-phase reactions. Surprisingly, the observational data reveals an enhanced production rate of secondary aerosols, suggesting an important contribution from other formation pathways, most likely heterogeneous reactions. These reactions appeared to be more efficient in producing secondary inorganics aerosols than organic aerosols resulting in a strongly elevated fraction of inorganics during heavily polluted periods. (4) Moreover, we found that high aerosol concentration was a regional phe-

nomenon. The accumulation process of aerosol particles occurred successively from cities southeast of Beijing. The apparent sharp increase in PM<sub>2.5</sub> concentration of up to several hundred  $\mu\text{g m}^{-3}$  per hour recorded in Beijing represented rapid recovery from an interruption to the continuous pollution accumulation over the region, rather than purely local chemical production. This suggests that regional transport of pollutants played an important role during these severe pollution events.

## 1 Introduction

Severe haze episodes in the winter of 2012–2013 engulfed Beijing, as well as other cities in southeastern China, causing one of the worst atmospheric pollution events in history. With hourly fine particle (PM<sub>2.5</sub>) concentrations up to  $\sim 900 \mu\text{g m}^{-3}$ , outdoor exposure caused adverse health effects (Nel, 2005; Pöschl, 2005; Peplow, 2014), including severe respiratory system related symptoms and deceases (Cao et al., 2014; Ouyang, 2013). Meanwhile the visibility was reduced down to 100 m, which disrupted traffic with can-

celed flights and closed highways. The government had to adopt emergency response measures to deal with these pollution episodes (<http://english.sina.com/china/p/2013/0113/548263.html>). In addition to massive amounts of primary particulate matter, high emissions in China provided plenty of gas pollutants to serve as precursors for secondary aerosols (Zhang et al., 2009). Densely distributed mega-cities (i.e., city clusters) have worsened this situation, contributing to regional air pollution. Once the regional pollution is formed, the advection becomes less effective in scavenging local pollutants (no clean air from upwind). Thus, the regional pollution is more persistent compared with air pollution within a specific city. Moreover, cities within this region could not eliminate their pollution solely by reducing local emissions (Chan and Yao, 2008; Cheng et al., 2008a).

These extreme haze episodes attracted great scientific interest. The visibility impairment has been attributed to scattering and absorption of solar radiation by aerosol particles (mostly  $\text{PM}_{2.5}$ ) and their hygroscopic growth under high relative humidity (Cheng et al., 2006, 2008b, c). Regional transport of pollutants was found to contribute considerably to concentrations of  $\text{PM}_{2.5}$  (Z. Wang et al., 2014; L. T. Wang et al., 2014), dust (Yang et al., 2013; Y. Wang et al., 2014), and  $\text{SO}_2$  (Yang et al., 2013) in Beijing. Atmospheric dynamic processes during hazy conditions were different from clean conditions, with a significant two-way feedback between  $\text{PM}_{2.5}$  and boundary layer evolution (Z. Wang et al., 2014). Secondary inorganic aerosol species were suggested to be the major contributor to severe haze, based on offline  $\text{PM}_{2.5}$  analysis (Quan et al., 2014), and online non-refractory  $\text{PM}_1$  analysis by an Aerosol Chemical Speciation Monitor (Sun et al., 2014). In addition, some studies described unusual atmospheric phenomena taking place under heavily polluted conditions, such as extremely low ozone concentration (less than 5 ppb) in the absence of diurnal variation (Zhao et al., 2013) and the synergistic oxidation of  $\text{SO}_2$  and  $\text{NO}_2$  (He et al., 2014). These findings suggest need for a better understanding on the haze formation mechanisms.

In this study, we address the following questions for the winter haze episodes aforementioned: (1) the relative importance of enhanced emission versus meteorology; (2) the cause of the sharp  $\text{PM}_{2.5}$  increase during the haze episodes in Beijing, whether it was mainly driven by an extremely rapid local chemical production or by regional transport; and (3) the dominant chemical mechanisms of haze formation.

## 2 Experimental methods

Online ambient observation was conducted from 1–31 January 2013 on the campus of Tsinghua University. The observation site is situated on the rooftop of the Environmental Science Building (40°00′17″ N, 116°19′34″ E), approximately 10 m above ground. Tsinghua University is located in the northwest part of urban Beijing, close to the North 4th

Ring Road, without any major pollution sources nearby. All observation data are hourly unified data.

Mass concentrations of fine ( $\text{PM}_{2.5}$ ) and coarse ( $\text{PM}_{2.5-10}$ ) particles were simultaneously measured based on the  $\beta$ -ray absorption method by a PM-712 Monitor (Kimoto Electric Co., Ltd., Japan), which was equipped with a US-EPA  $\text{PM}_{10}$  inlet and a  $\text{PM}_{2.5}$  virtual impactor (Kimoto Electric Co., Ltd., 2012; Kaneyasu et al., 2014). Dehumidification was achieved with the hygroscopic growth correction formula:

$$\begin{aligned} & \text{Dehumidified } \text{PM}_{2.5} \text{ mass conc.} \\ &= \text{Measured } \text{PM}_{2.5} \text{ mass conc.} \times \frac{1}{1 + 0.010 \times e^{6.000 \frac{\text{RH}}{100}}}, \end{aligned} \quad (1)$$

where the 0.010 and 6.000 are localized coefficients, and RH is relative humidity in %. All  $\text{PM}_{2.5}$  hereinafter refer to the dehumidified  $\text{PM}_{2.5}$  data.

A Sunset Model 4 Semi-Continuous Carbon Analyzer (Beaverton, OR, USA) was used to measure hourly organic carbon (OC) and elemental carbon (EC) concentrations in  $\text{PM}_{2.5}$ . A NIOSH (National Institute for Occupational Safety and Health) temperature protocol was used and the calculation discrepancy under high ambient concentrations was corrected accordingly (G.J. Zheng et al., 2014). Organic matter (OM) was estimated as 1.6·OC, based on previous results (Zhang et al., 2014; Xing et al., 2013). The use of fixed OM/OC ratio requires caveats because the ratio might change due to the variable oxidation degree of OM under different conditions.

Hourly sulfate and nitrate concentrations in  $\text{PM}_{2.5}$  were measured using an ACSA-08 Monitor (Kimoto Electric Co., Ltd., Japan). The ACSA-08 Monitor measured nitrates using an ultraviolet spectrophotometric method, and quantified sulfates with the  $\text{BaSO}_4$ -based turbidimetric method after addition of  $\text{BaCl}_2$  dissolved in polyvinyl pyrrolidone solution (Kimoto et al., 2013). Ammonium was predicted under the assumption that it existed as  $\text{NH}_4\text{NO}_3$  and  $(\text{NH}_4)_2\text{SO}_4$  (He et al., 2012), which might be an overestimation based on the non-refractory  $\text{PM}_1$  results (Sun et al., 2014). Thus the predicted ammonium given here should be regarded as an upper limit.

An automatic meteorological observation instrument (Milo520, VAISALA Inc., Finland) was used to obtain meteorological parameters, including atmospheric pressure, temperature, RH, wind speed, and wind direction. Specific humidity was calculated from these measured parameters (<http://www.srh.noaa.gov/epz/?n=wxcalc>).

$\text{SO}_2$  and  $\text{NO}_2$  concentrations in Beijing, and  $\text{PM}_{2.5}$  concentrations in other cities were acquired from the Atmospheric Environment Monitoring Network (Tang et al., 2012). Daily averaged solar radiation reaching ground data were downloaded from the China Meteorological Data Sharing Service System (<http://cdc.cma.gov.cn>). Planetary boundary layer (PBL) height was simulated with the Weather

Research & Forecasting (WRF) Model (B. Zheng et al., 2014).

### 3 General characteristics of Beijing winter haze

Primary atmospheric pollutant in Beijing during the winter of 2012–2013 was  $\text{PM}_{2.5}$ , which constituted about 70 % of  $\text{PM}_{10}$ . This ratio increased when  $\text{PM}_{2.5}$  pollution became worse (Fig. 1b). Monthly average  $\text{PM}_{2.5}$  concentration reached  $121.0 \mu\text{g m}^{-3}$  in January 2013, and hourly  $\text{PM}_{2.5}$  concentrations peaked at  $855.10 \mu\text{g m}^{-3}$ , which was the highest ever reported in Beijing (Zhao et al., 2009, 2011, 2013; Zhang et al., 2014). The severe  $\text{PM}_{2.5}$  pollution lasted nearly the whole month, characterized by frequent and long-lasting pollution episodes. Here, we define an episode as a set of continuous days with daily  $\text{PM}_{2.5}$  averages exceeding  $75 \mu\text{g m}^{-3}$ . In total, four episodes were identified in January 2013 (Fig. 1a): 4–8 January (Episode I), 10–16 January (Episode II), 18–23 January (Episode III), and 25–31 January (Episode IV). Maximum episode-averaged  $\text{PM}_{2.5}$  concentrations reached  $245.4 \mu\text{g m}^{-3}$  in Episode II (see Table 1 for comparative information on Episodes I to III; Episode IV was not included because of missing data). In addition to the high average concentrations, these episodes were frequent (intervals between episodes were all  $\sim 1$  day) and long-lasting (5–7 days) compared with typical durations (5 days) and frequencies (1–3 days) of previous Beijing winter haze episodes (Jia et al., 2008).

Another unique feature of the  $\text{PM}_{2.5}$  mass concentrations during this winter haze period was their dramatic hourly fluctuation. The maximum daily variation was  $778.6 \mu\text{g m}^{-3}$  on 12 January. Hourly  $\text{PM}_{2.5}$  changes of over  $100 \mu\text{g m}^{-3}$  (increases or decreases) were observed over 40 times during this haze period. Hourly increases or decreases could reach up to  $351.8 \mu\text{g m}^{-3}$  and  $-217.7 \mu\text{g m}^{-3}$ , respectively. Causes of these sharp transitions are discussed in Sect. 5.

The variation of chemical composition with  $\text{PM}_{2.5}$  pollution level, and among episodes, was also explored. We classified  $\text{PM}_{2.5}$  pollution into four categories according to the Air Quality Index ([http://kjs.mep.gov.cn/hjbhzbz/bzwb/dqjhjh/jcgfffbz/201203/t20120302\\_224166.htm?COLLCC=2906016564&](http://kjs.mep.gov.cn/hjbhzbz/bzwb/dqjhjh/jcgfffbz/201203/t20120302_224166.htm?COLLCC=2906016564&)) (Fig. 1b): clean ( $\text{PM}_{2.5} \leq 35 \mu\text{g m}^{-3}$ ), slightly polluted ( $35 < \text{PM}_{2.5} \leq 115 \mu\text{g m}^{-3}$ ), polluted ( $115 < \text{PM}_{2.5} \leq 350 \mu\text{g m}^{-3}$ ), and heavily polluted ( $\text{PM}_{2.5} > 350 \mu\text{g m}^{-3}$ ), where  $\text{PM}_{2.5}$  refers to the hourly concentration. Under this classification, the slightly polluted, polluted, and heavily polluted levels generally correspond to small, moderate, and large  $\text{PM}_{2.5}$  peaks in Fig. 1b. Mean percentile compositions of major components in  $\text{PM}_{2.5}$  under different pollution levels were shown in Fig. 2a. With increasing pollution level, the EC fraction decreased slightly, OC fraction decreased significantly, while sulfate and nitrate contributions increased sharply (Fig. 2a). It suggests that secondary inorganic aerosol species become more important

during polluted periods concerning their contribution to the  $\text{PM}_{2.5}$ . A similar trend was observed for NR- $\text{PM}_{10}$  (Sun et al., 2014) and off-line samples (Cheng et al., 2015). On average, OC, EC, nitrate, and sulfate comprised 21, 3, 19 and 22 % of  $\text{PM}_{2.5}$  (Fig. 2b). Good correlations with  $\text{PM}_{2.5}$  were observed for OC, EC and nitrate ( $R^2 > 0.8$  for these three species) for all data in January 2013, while for sulfate the correlation became weaker, reflecting larger episodic variations (Fig. 2b). In Episode III,  $\text{NO}_2$  exceeded  $\text{SO}_2$  by 50 % (Table 1), generally in accordance with previous studies (Meng et al., 2009). In contrast, concentration of  $\text{SO}_2$  exceeded  $\text{NO}_2$  in Episodes I and II. Compared with Episode II, Episode I was much drier, which is unfavorable to the sulfate formation. The relatively high  $\text{SO}_2$  but low  $\text{NO}_2$  concentrations in Episodes I and II may indicate the significance of stationary sources (coal combustion, etc.) in local emissions or regional  $\text{SO}_2$ -rich air masses transported to Beijing.

### 4 Emission enhancement vs. synoptic conditions

Haze episodes were much more severe and frequent in winter 2013 than in 2012. One possible explanation is that there was an abrupt emission enhancement during 2013. However, we didn't find such change in the emission inventory (<http://www.meicmodel.org/>). Annual average emissions of primary  $\text{PM}_{2.5}$ ,  $\text{SO}_2$  and  $\text{NO}_x$  show slight differences between 2013 and 2012 (1.2,  $-1.3$  and 0.8 %, respectively) for the Beijing–Tianjin–Hebei region. The changes of monthly averaged emissions in January were higher than the annual average changes in rates, i.e., 2.1, 1.5 and 2.5 % for primary  $\text{PM}_{2.5}$ ,  $\text{SO}_2$ , and  $\text{NO}_x$ , respectively; but they are still not significant compared to the changes in pollutant concentrations. Thus, we suspect that these haze episodes arose from the unfavorable synoptic conditions in January 2013.

The relative importance of enhanced emission versus unfavorable meteorology in  $\text{PM}_{2.5}$  concentration of January 2013 was estimated by model simulations with three scenarios (Fig. 3). Base scenario (a) was designed to simulate the actual situation, i.e., with both input emission inventory and meteorology for January 2013. In scenarios (b) and (c), January 2012 meteorology and January 2012 emission inventory data were used, respectively. Since the original WRF-CMAQ (Weather Research and Forecasting – Community Multiscale Air Quality) modeling system cannot reproduce the observed concentrations under heavily polluted conditions (B. Zheng et al., 2014), a revised WRF-CMAQ system with enhanced heterogeneous reactions (Wang et al., 2012) was adopted to improve the model performance. The revised model could effectively capture the measured concentrations of total  $\text{PM}_{2.5}$  (with normalized mean biases (NMBs) being 0.4 %) and its different chemical compositions for both clean and heavily polluted haze days (B. Zheng et al., 2014). Details of the

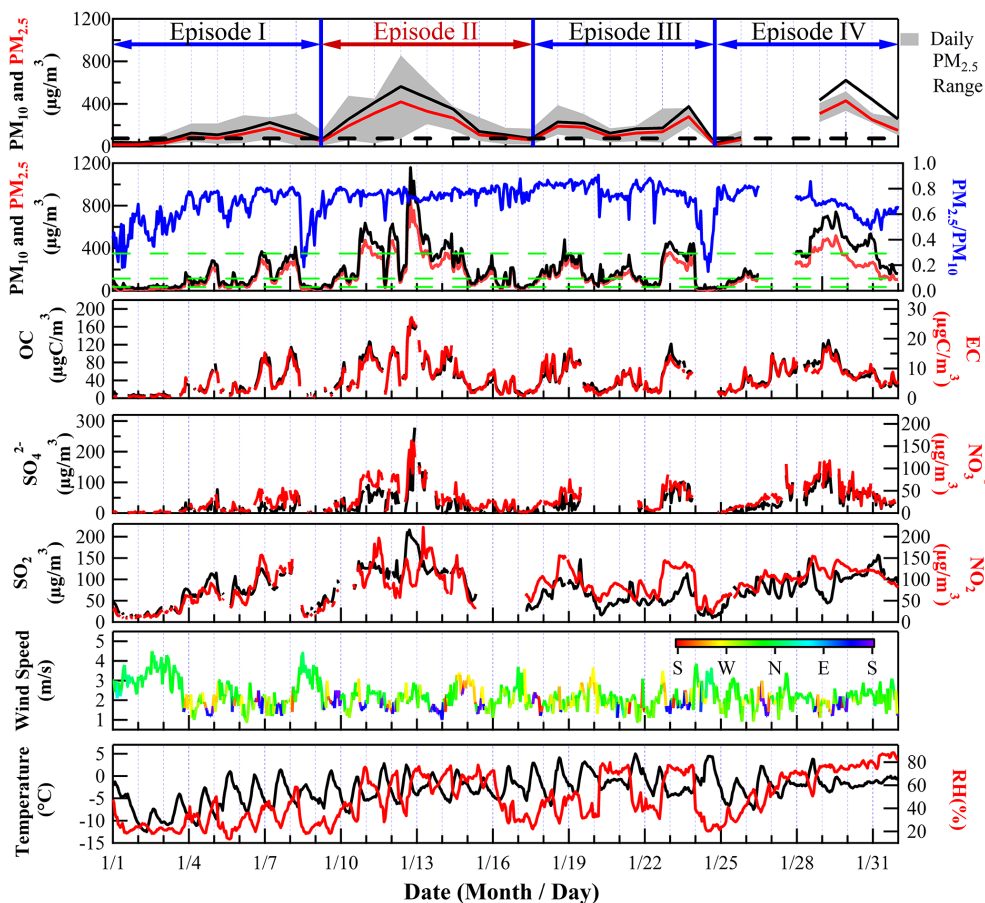


**Figure 1.** Time series of PM<sub>10</sub>, PM<sub>2.5</sub>, and its major components (OC, EC, SO<sub>4</sub><sup>2-</sup> and NO<sub>3</sub><sup>-</sup>), and meteorological data (wind speed, wind direction, temperature and relative humidity) for January 2013.

**Table 1.** General information on severe haze episodes in January 2013.

		Episode I			Episode II			Episode III			January		
		Ave.	min	max	Ave.	min	max	Ave.	min	Max	Ave.	min	max
Meteorology data	Temperature (°)	-4.63	-11.10	1.40	-2.79	-8.30	2.80	-1.26	-6.60	5.00	-2.94	-12.50	5.00
	RH(%)	31.16	13.50	58.50	56.59	27.20	77.60	55.05	27.10	79.70	47.97	13.50	88.30
	WS(m s <sup>-1</sup> )	2.10	0.90	4.40	2.08	1.00	3.40	1.96	0.90	3.60	2.18	0.90	4.50
PM <sub>2.5</sub> and PM <sub>10</sub>	PM <sub>2.5</sub> ( $\mu\text{g}/\text{m}^3$ )	112.50	11.00	311.50	245.37	21.10	855.10	167.66	35.40	387.30	161.77	4.40	855.10
	PM <sub>10</sub> ( $\mu\text{g}/\text{m}^3$ )	152.17	28.80	411.00	327.17	31.60	1157.50	214.03	41.50	479.80	223.53	13.90	1157.50
	PM <sub>2.5</sub> /PM <sub>10</sub> (%)	0.69			0.75			0.79			0.70		
Gas data	NO <sub>2</sub>	76.39			109.44			95.86			86.09		
	SO <sub>2</sub>	79.73			123.35			63.86			77.54		

model configuration, modifications, and validation are described in B. Zheng et al. (2014).

As expected, the influence of emission difference was negligible (Fig. 3a and 3c). For the whole simulation domain of the North China Plain (NCP), both simulation with January 2012 meteorology (Scenario (c) and January 2013 meteorology (Scenario (a) resulted in similar PM<sub>2.5</sub> concentration ranges ( $\sim 50$  to  $\sim 500 \mu\text{g}/\text{m}^3$ ) and spatial distributions. Difference of PM<sub>2.5</sub> concentration at any site was

within  $\pm 10 \mu\text{g}/\text{m}^3$  (Fig. 3e). Simulation results of Scenario (a) and (c) were not only similar in average concentration levels, but also in temporal variations. For example, in Beijing, simulated hourly PM<sub>2.5</sub> concentration results under this two scenarios presented not only similar concentration (being  $279.1 \pm 170.2 \mu\text{g}/\text{m}^3$  and  $278.8 \pm 168.9 \mu\text{g}/\text{m}^3$ , respectively) but also excellent correlation with  $R^2$  reaching 0.97.

In contrast, stable synoptic conditions in January 2013, which favored accumulation of emitted pollutants, were es-

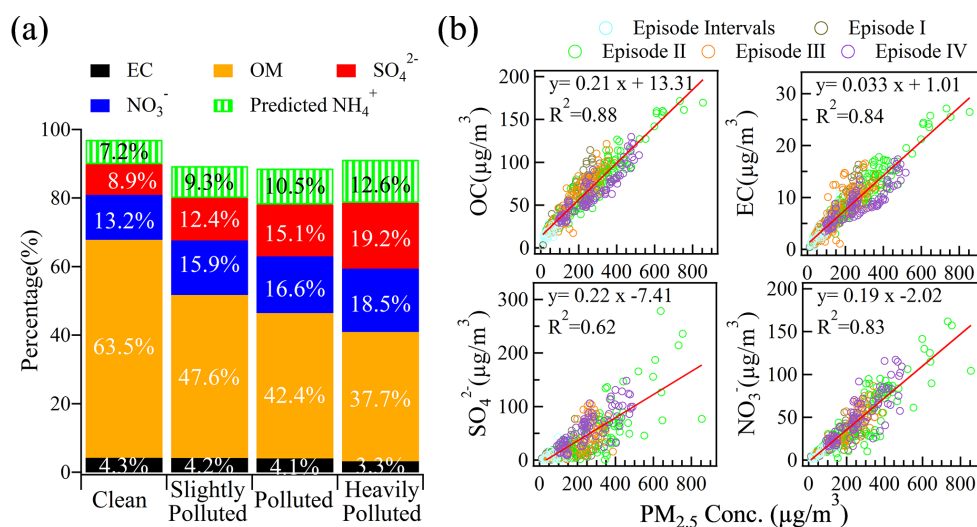


**Figure 2.** Major composition of PM<sub>2.5</sub> with respect to pollution level. **(a)** Mean percentile composition and **(b)** hourly concentration of individual species plotted against PM<sub>2.5</sub> mass concentration. Values showed in **(a)** were derived as average of ratios.

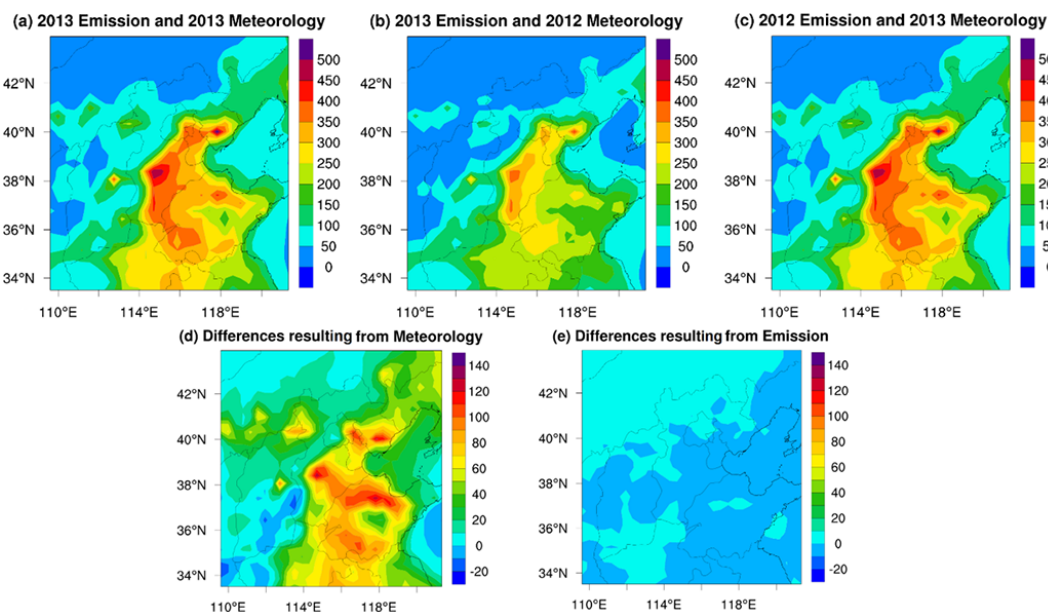


**Figure 3.** Revised WRF-CMAQ simulated monthly averaged PM<sub>2.5</sub> concentration (μg m<sup>-3</sup>) under different scenarios. **(a)** Base scenario. Actual January 2013 emission and January 2013 meteorology data were used. **(b)** January 2012 meteorology data were used, and **(c)** January 2012 emissions were used. The different PM<sub>2.5</sub> concentrations (μg m<sup>-3</sup>) caused by meteorology **(d)**; equivalent to **a–b**) and emission **(e)**; equivalent to **a–c**) are also shown.

essential to the formation of the severe regional haze. Under the same emission level, changing the meteorological conditions from 2012 to 2013 resulted in a monthly average PM<sub>2.5</sub> increase of 10–40 μg m<sup>-3</sup> in the Beijing area, and up to 120 μg m<sup>-3</sup> over the whole NCP (Fig. 3a, b, d). This suggests that the severe haze episodes in January 2013 were most likely due to unfavorable meteorology, rather than an abrupt increase in emissions (Fig. 3d, e).

Figure 4 compares peak PM<sub>2.5</sub> concentrations in the NCP region during Episodes II to IV and their corresponding surface weather maps, together with surface weather map from a clean hour (Fig. 4g). During severe haze episodes, the regional pollution covered most of the Hebei and northern Henan provinces. In general, Shandong Province was less polluted, except during Episode IV. Beijing borders this polluted region with mountains to the northwest. Surface weather maps from polluted periods were generally char-

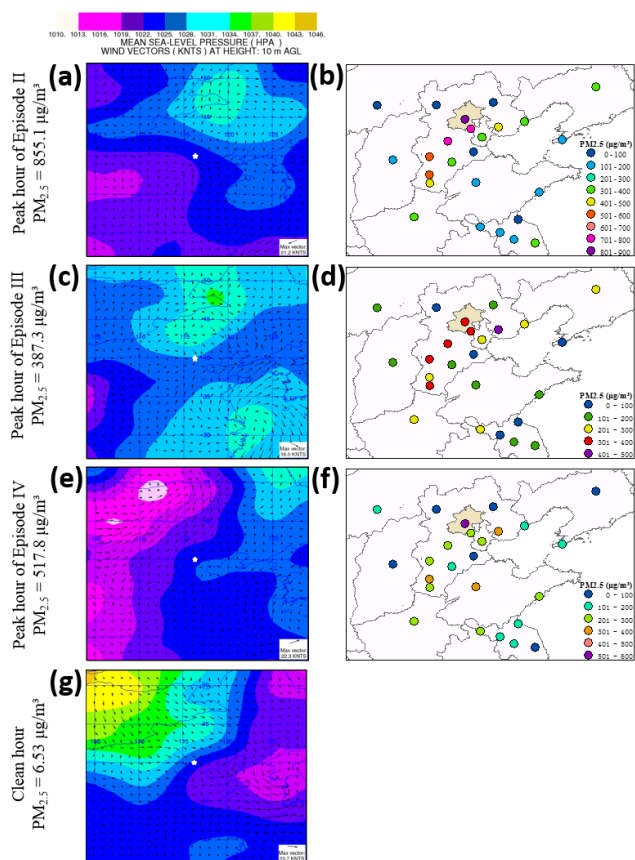


**Figure 4.** Surface weather maps (a, c, e, g) and  $\text{PM}_{2.5}$  concentrations (b, d, f) of the North China Plain on 12 January LT 18:00 (a, b), 18 January LT 20:00 (c, d), 29 January LT 13:00 (e, f), and 1 January LT 08:00 (g). The location of Beijing is indicated as a white star on the weather maps, and as the shaded area on the  $\text{PM}_{2.5}$  concentration maps.  $\text{PM}_{2.5}$  concentrations in Beijing at the four selected time points are also shown on the left for reference.

acterized by a weak high-pressure center (1034–1037 hPa) northeast of Beijing, which could result in low surface wind speed and prevent the influx of northwest clean air (Xu et al., 2011; Zhao et al., 2013). During the peak hours of Episode II, Beijing was located near a low-pressure trough, where air masses from south, west and northeast converged. During Episode III, Beijing was located in a saddle between two pairs of high- and low-pressure centers, which also led to enhanced stability. In contrast, weather patterns for the clean hours were characterized by strong high-pressure centers (up to 1046 hPa) northwest of Beijing, i.e., the Siberian anticyclone. With sharp pressure gradient, synoptic conditions produce effective convection and strong northerly winds, bringing dry and clean air masses into Beijing.

Local meteorology, controlled by synoptic conditions, could have “deterministic impacts” on air pollution levels (Xu et al., 2011). Compared with the clean periods, the polluted periods were associated with significantly lower wind

speed and PBL, and higher temperature and RH (Fig. 5). Besides changes in the average level, diurnal pattern of temperature in polluted periods could also differ from clean periods, with diminished overnight (00:00 to 06:00 a.m.) temperature drop.

## 5 Local chemical production vs. regional transport

As shown in Fig. 6, Episode II consists of several sharp-increase events, in which  $\text{PM}_{2.5}$  concentrations increased by over  $400 \mu\text{g m}^{-3}$  within 1–3 hours (maximum mass growth rate up to  $351.8 \mu\text{g m}^{-3} \text{h}^{-1}$ ). Earlier studies have attributed this dramatic rate of increase to fast local chemical production (Y. Wang et al., 2014). However, we found that the apparent rapid changes are more likely to be caused by the regional transport of clean/polluted air masses. In winter, the Siberian anticyclone could bring clean air masses into NCP (Jia et al., 2008; Liu et al., 2013) while southerly winds refill the areas with polluted air masses. The transition between clean and polluted air masses may result in an apparent sharp build-up of particle concentrations. In other words, these events reflected interruption and rapid recovery of pollution from adjacent areas, rather than merely local chemical production.

The impact of transport is supported by the temporal variations in the regional distribution of  $\text{PM}_{2.5}$  concentrations, the surface weather maps, and the specific humidity (Fig. 6 and 7). The first evidence is that these sharp  $\text{PM}_{2.5}$  build-up events were unique to Beijing among all the eight cities around/in the NCP (Fig. 6). Chengde and Zhangjiakou are situated to the north of NCP with mountains in between (Fig. 6a). Among the NCP cities, Beijing is located at the northern tip, with mountains to the north and west shielding the city (Fig. 6(a2)). When conditions favor transport of clean air from north or northwest (i.e., with the advent of a cold air current), Beijing is the first one among NCP cities to be scavenged, which resulted in a sharp drop of  $\text{PM}_{2.5}$  concentrations. In this case,  $\text{PM}_{2.5}$  levels in Beijing became similar to the upwind cities, i.e., Chengde and Zhangjiakou (yellow solid circles; Fig. 6(b1)). However, these cold air currents were too weak to go further, leaving the rest NCP cities unaffected. Not surprisingly, the influence of these weak cold air currents soon receded and the polluted air parcels were transported back to Beijing, which lead to a sharp increase in the  $\text{PM}_{2.5}$  level similar as the rest NCP cities (e.g., Shijiazhuang, Baoding, Tianjin, Langfang, and Tangshan) (yellow solid circles; Fig. 6(b2 and b3)).

In accordance with the above description, surface weather maps showed that the sharp  $\text{PM}_{2.5}$  increase/decrease events in Beijing during January 2013 were always accompanied with quick transition between low/high pressure systems. As shown in Fig. 7b, the two sharp drops in  $\text{PM}_{2.5}$  concentration on 11 and 12 January corresponded to a weak high-pressure system developed in the mountains northwest of

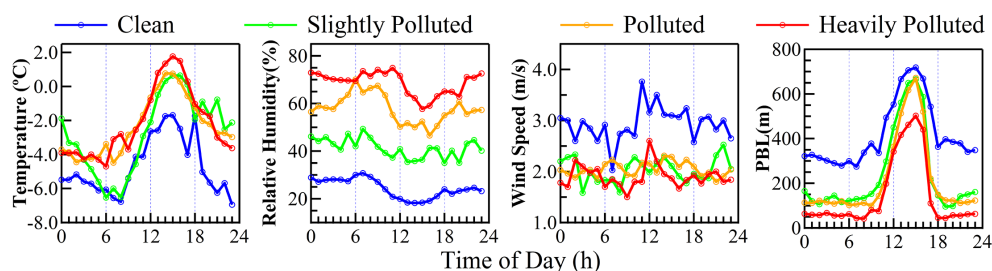


**Figure 5.** Mean diurnal variation in meteorological parameters for different pollution levels.

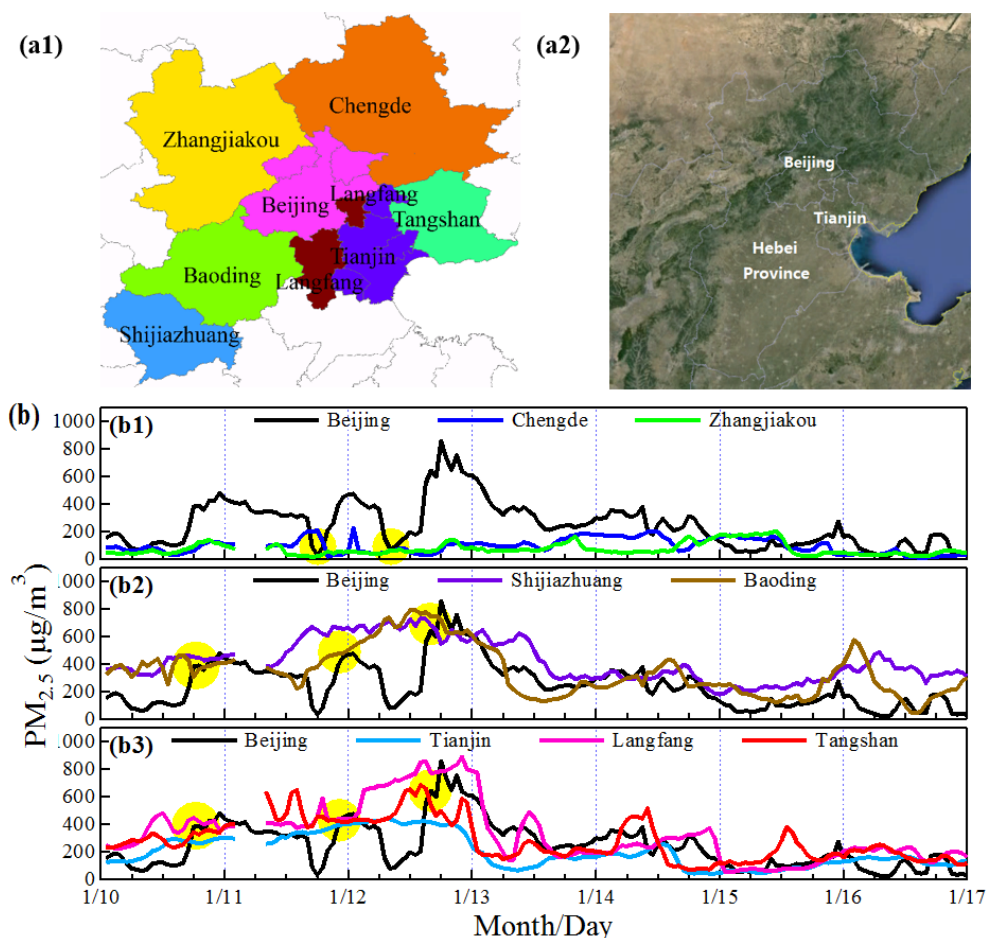


**Figure 6.** (a1) The location of all cities shown below, and (a2) topographic map around Beijing. (b)  $PM_{2.5}$  concentrations of Beijing and its (b1) northern cities, (b2) southwest cities, and (b3) southeast cities for the period 10–17 January 2013. Yellow solid circles indicated the time periods when the sharp drops (b1) and sharp increases (b2 and b3) of  $PM_{2.5}$  concentration occurred.

Beijing, which brought clean air mass into the city. When the high-pressure systems diminished, a low-pressure system developed southwest of Beijing, and the air mass in Beijing was again affected by the regional background pollution, resulting in a sharp increase in  $PM_{2.5}$  concentration.

The observed variation of the specific humidity, an indicator for the origin of air masses (Jia et al., 2008), also supports our explanation (Fig. 7a). Air masses from the south

were usually warmer and wetter than the northern air masses, thus possessing a higher specific humidity. During the rapid changes of  $PM_{2.5}$ , the trend of specific humidity nicely followed the variations of  $PM_{2.5}$  (Fig. 7a, pink and yellow rectangles marked periods), which reflected the quick transition of air parcel origins. It has been suggested that the decrease of PBL height will compress air pollutants into a shallow layer, resulting in elevated pollution levels (Liu et

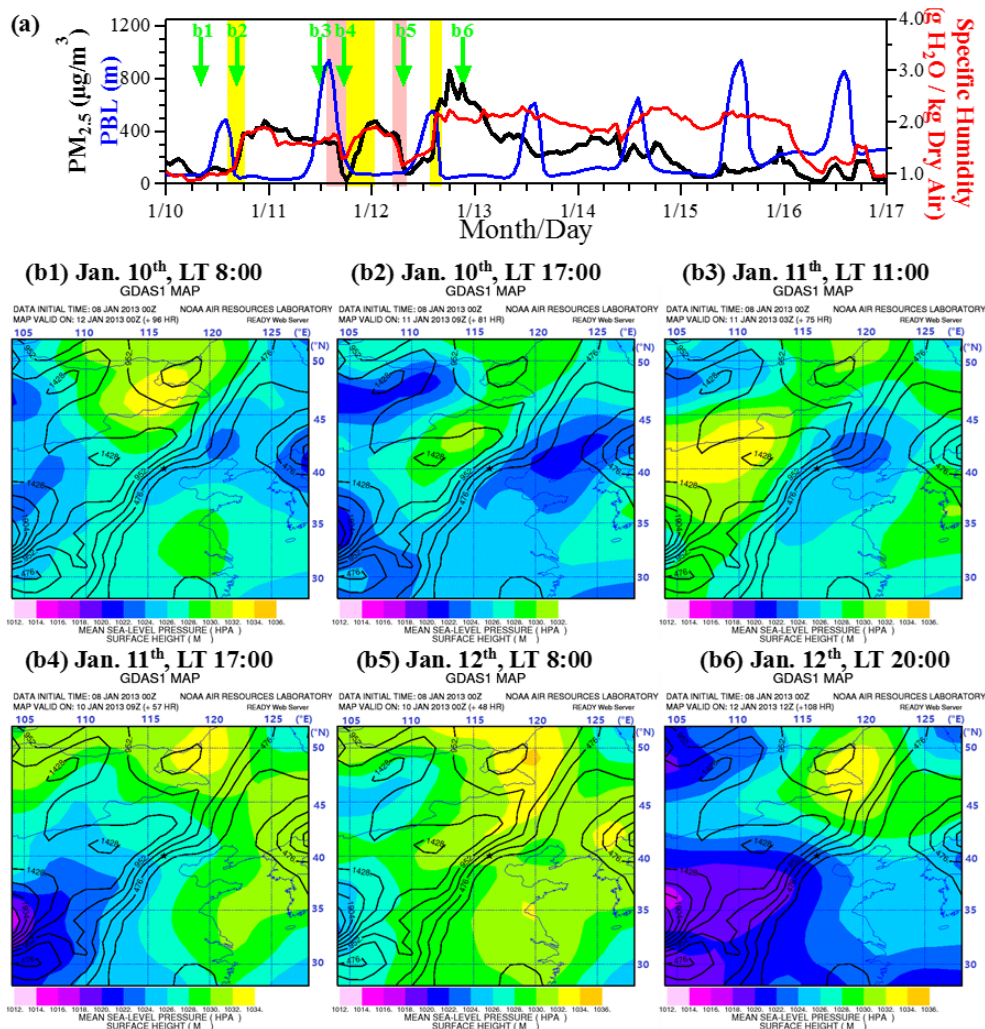


**Figure 7.** Evidence for regional transport of pollutants as a major factor contributing to sharp concentration increases in Beijing. (a)  $\text{PM}_{2.5}$  concentration, PBL height, and specific humidity in Beijing for 10–17 January 2013. Pink and yellow rectangles indicated the sharp drop and sharp increase periods of  $\text{PM}_{2.5}$ , respectively. Note how nicely specific humidity and  $\text{PM}_{2.5}$  followed each other during these periods. (b) Weather patterns before and after the sharp increases events. Corresponding time point of (b1) to (b6) was indicated by arrows in (a). The topography map (elevation) is also shown for reference. Location of Beijing was indicated by the black star in center of each graph.

al., 2013). However, our results indicated that the compression was not really happening. Rather, the decrease of PBL height hindered the vertical mixing of pollutants, resulting in a faster accumulation and higher concentrations. As shown in Fig. 7a, the time lag between variations in PBL and its effects on  $\text{PM}_{2.5}$  concentration is a clear evidence demonstrating that the PBL was not “compressing” air pollutants into a shallower layer. Otherwise, concurrent increase in  $\text{PM}_{2.5}$  will be found during the decrease of PBL height.

## 6 Formation of secondary aerosols

Compared with clean conditions, the hazy days are characteristic of weaker radiation and higher RH. The RH depends on

the synoptic conditions while the radiation reduction is due to the direct radiative effects of aerosol particles (Crutzen and Birks, 1982; Ramanathan and Carmichael, 2008; Ramanathan et al., 2001; Cheng et al., 2008b; Wendisch et al., 2008). Secondary aerosols (inorganic and organic) are major components in fine particles in China (Yang et al., 2011). In this section, we will evaluate the impact of changes in radiation and RH on the formation of secondary aerosols.

To evaluate the role of chemical productions, we analyzed the EC-scaled concentrations for individual compounds. The purpose of using EC-scaled concentration is to eliminate the influence of different dilution/mixing conditions on the variation of observed pollutant concentrations. The observed variations of pollutant concentrations are not only controlled by the chemical reactions but are also subject to the influence

of boundary layer developments. For the same emission rate and chemical production rate, different mixing conditions will result in different levels of air pollutants. It is thus highly uncertain to conclude a stronger/weaker chemical production based on purely concentration data without considering the boundary layer effect. Since EC is an aerosol species coming from only primary emission and quite inertial to chemical reactions, its variations well reflect the influence of atmospheric physical processes (dilution/mixing effect). The ratio of other species to EC will to a large extent eliminate the variations due to mixing/dilution and better represent the contribution from chemical reactions.

### 6.1 Weakened importance of photochemistry

The radiative reduction imposed by aerosol particles is particularly strong during haze episodes because of extremely high particle concentrations. Take Beijing for example: during haze episodes, the amount of solar radiation reaching the ground was significantly lower (e.g., down to  $2.77 \text{ MJ m}^{-2} \text{ d}^{-1}$ , 13 January) than it was on clean days (averaging  $9.36 \pm 0.60 \text{ MJ m}^{-2} \text{ d}^{-1}$  for all the 6 clean days), rendering high photochemical activity impossible. The reduction of radiation intensities will change the atmospheric photochemistry and oxidant concentrations (hydroxyl radical (OH) and ozone ( $\text{O}_3$ )), which will consequently change the production and aging of secondary organic aerosols (SOAs) (Hallquist et al., 2009; Jimenez et al., 2009).

As the haze pollution spread over most of the NCP, a weakening of photochemistry was expected on the regional scale, which is confirmed by both observations and model simulations. Extremely low ozone concentration (less than 10 ppb) in the absence of diurnal variation was observed during heavy pollution episodes for all of the three major cities in Jing–Jin–Ji Area (i.e., Beijing, Tianjin and Shijiazhuang) in January 2013 (Y. Wang et al., 2014). Similar phenomenon was observed before in another heavy pollution episode in winter Beijing (Zhao et al., 2013). In accordance with the observed low ozone concentration, model simulations also showed a regional-scale reduction in the concentrations of ozone and OH (Fig. 8). Average daytime concentrations of oxidants were significantly lower during polluted periods than clean periods. For most areas in the NCP,  $\text{O}_3$  and OH dropped from  $12 \sim 44 \text{ ppbV}$  and  $0.004 \sim 0.020 \text{ pptV}$  to less than  $12 \text{ ppbV}$  and  $0.004 \text{ pptV}$ , respectively, as the air quality changed from clean to heavily polluted conditions. This regional drop in oxidant concentrations demonstrates the impact of air pollution on the photochemistry.

Ozone and OH radicals are known as crucial oxidants in the formation of secondary organics aerosols (SOAs) (Jimenez et al. 2009). Weakened photochemistry is therefore expected to reduce the SOA production and concentrations. To have a semi-quantitative estimation on the contribution of photochemistry, secondary organic carbon (SOC) was estimated (Fig. 9a) using the EC-tracer method (Lim and Turpin,

2002). Briefly, SOC was estimated using these formulae:

$$\text{Primary OC} = \text{EC} \cdot (\text{OC/EC})_{\text{pri}} + N \quad (2)$$

$$\text{SOC} = \text{OC} - \text{Primary OC} \quad (3)$$

The basic assumptions and underlying principles of this method are discussed in Lim and Turpin (2002) and Lin et al. (2009). Only daytime (07:00–18:00) carbonaceous aerosol data were used here to exclude possible interference from day–night source variations (such as the heavy-duty diesel truck traffic which is allowed only during nighttime in Beijing). In our study, data pairs with the lowest 10 % percentile of ambient OC/EC ratios were used to estimate the primary OC/EC ratio (Fig. 9a). York regression (York et al., 2004) was used to estimate the intercept  $N$  and the slope, i.e., values of  $(\text{OC/EC})_{\text{pri}}$ , according to Saylor et al. (2006). Our analysis shows that SOC constituted  $\sim 28 \%$  of total OC, consistent with earlier studies in the winter of 2009–2012 ( $\sim 30 \%$ , Cheng et al., 2011; Sun et al., 2013b).

High concentration of aerosol particles can reduce solar radiation and atmospheric photochemistry. Since SOC is a product of photochemical reactions, we would expect a reduced SOC production rate under heavily polluted conditions. This is confirmed by the measured SOC concentrations shown in Fig. 9. Here again the EC-scaled SOC was used to account for the different boundary layer effect (dilution/mixing) on the aerosol concentrations. Both SOC/EC and the accumulated SOC/EC (afternoon – morning values) decrease when it changed from clean to heavily polluted periods. The accumulated SOC/EC is used to better represent the production during the daytime.

Reduction in photochemistry-related  $\text{PM}_{2.5}$  production is further supported by model simulation results. In our model configurations, the photolysis rate is calculated online using simulated aerosols and ozone concentrations (B. Zheng et al., 2014). As a result, with the enhanced  $\text{PM}_{2.5}$  concentration, the photolysis rate will be reduced, and so will the concentrations of photochemical oxidants (Fig. 8) and secondary aerosol particles. During the haze events, this effect can be counteracted by the enhanced heterogeneous reactions and it is difficult to unravel them from the measurement data.

In order to demonstrate the influence of reduced photochemistry, we adopted the original WRF-CMAQ model setup and excluded the enhanced heterogeneous reactions. In this case, only gas-phase oxidations are counted for the formation of sulfate and organics (aqueous-phase reactions in the original WRF-CMAQ only happen in clouds and don't apply for the aerosol phase) (B. Zheng et al., 2014) and their simulated concentrations will directly reflect the influence of reduced photochemistry. As shown in Table S1, the simulated  $\text{PM}_{2.5}/\text{EC}$  ratios decreased from 16.05 to 11.72 when the pollution level changed from the clean to the heavily polluted case, reflecting the reduced gas-phase photochemical production. Note that  $\text{PM}_{2.5}$  concentration is normalized by EC to counteract the influence of reduced boundary layer.

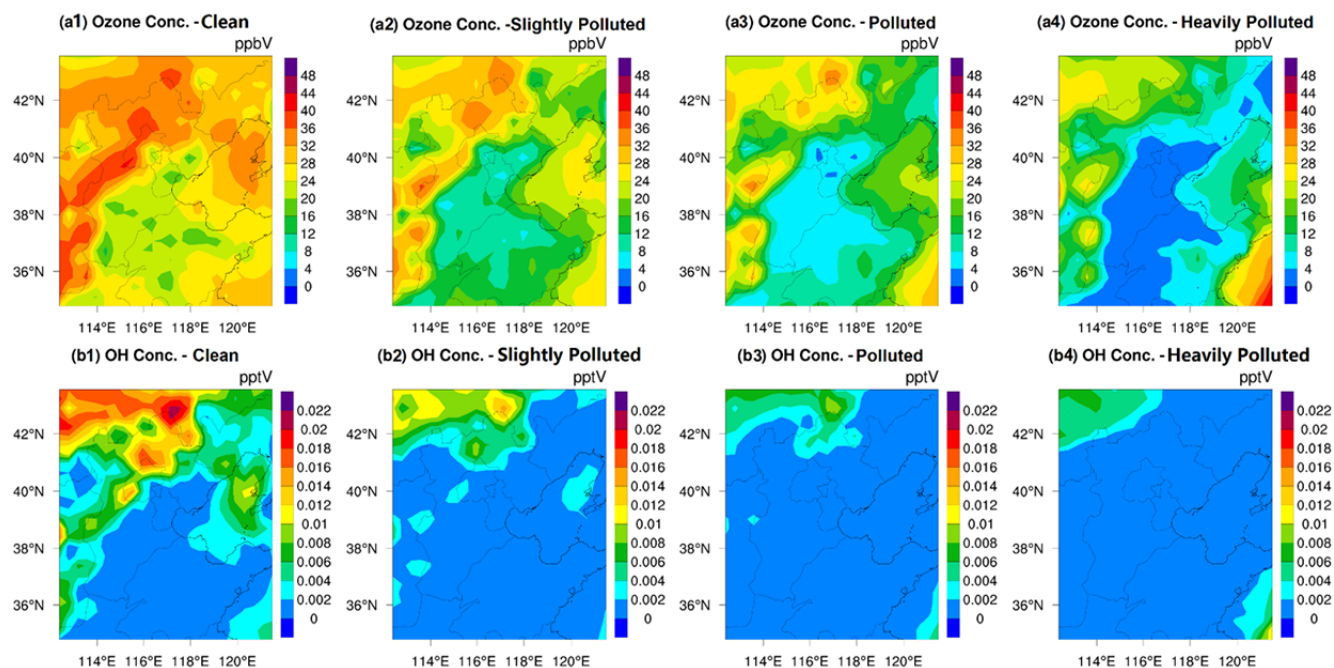


**Figure 8.** Revised WRF-CMAQ simulated regional distribution of daytime (07:00 ~ 18:00) concentration of (a)  $\text{O}_3$  (ppbV) and (b) OH (pptV) at different pollution level.

Otherwise, the reduced boundary layer itself could lead to a tremendous increase in the pollutant concentration under heavily polluted conditions, and thus cover the real effect of reduced photochemistry.

The simulated individual components of  $\text{PM}_{2.5}$  also reflected the influence of photochemistry. As shown in Table S1, although primary organic matter (POM) to EC ratios kept nearly constant during all pollution levels, the normalized secondary species all showed a decreasing trend, reflecting the reduced photochemical production.  $\text{SOA}/\text{EC}$ ,  $\text{SO}_4^{2-}/\text{EC}$ , and  $\text{NO}_3^-/\text{EC}$  ratios decreased by 53.3, 51.9 and 28.6 %, respectively from clean to heavily polluted periods. For the formation of  $\text{NO}_3^-$ , two heterogeneous reactions have been included in the original WRF-CMAQ model and therefore the  $\text{NO}_3^-/\text{EC}$  shows relatively less reduction than  $\text{SOA}/\text{EC}$  and  $\text{SO}_4^{2-}/\text{EC}$ .

## 6.2 Enhanced heterogeneous chemistry

Unlike OM, relative contributions of sulfate and nitrate to  $\text{PM}_{2.5}$  were increasing during the haze events (Fig. 2). Again, we used their ratios to EC to account for the boundary layer effect. An increasing trend of  $\text{SO}_4^{2-}/\text{EC}$  and  $\text{NO}_3^-/\text{EC}$  ratios was found (Column 1 in Fig. 10) from clean periods (3.03 and 3.33, respectively) to heavily polluted periods (6.35 and 5.89, respectively), suggesting enhanced chemical productions. The SOR and NOR (molar ratio of sulfate or nitrate to sum of sulfate and  $\text{SO}_2$  or nitrate and  $\text{NO}_2$ ) have been used as indicators of secondary transformation (Sun et al., 2006).

The fact that SOR and NOR increased much more rapidly than  $\text{SO}_2$  and  $\text{NO}_2$  as pollution events became more severe (Column 4 in Fig. 10) is further evidence of elevated secondary formations of sulfate and nitrate during severe haze events.

Both gas-phase and heterogeneous reactions could contribute to the formation of sulfate and nitrate from  $\text{SO}_2$  and  $\text{NO}_2$ , thus elevating the SOR and NOR. Sulfate is formed through oxidation of  $\text{SO}_2$  by gas-phase reactions with OH (Stockwell and Calvert, 1983; Blitz et al., 2003) and stabilized Criegee intermediate (which is formed by  $\text{O}_3$  and alkenes) (Mauldin et al., 2012), and by heterogeneous reactions with dissolved  $\text{H}_2\text{O}_2$  or with  $\text{O}_2$  under the catalysis of transition metal (Seinfeld and Pandis, 2006). Nitrate formation is dominated by the gas-phase reaction of  $\text{NO}_2$  with OH during daylight, and the heterogeneous reactions of nitrate radical ( $\text{NO}_3$ ) during nighttime (Seinfeld and Pandis, 2006). Since gas-phase production of secondary aerosols is expected to decrease under heavily polluted periods (Sect. 6.1), the increase of  $\text{SO}_4^{2-}/\text{EC}$  and  $\text{NO}_3^-/\text{EC}$  ratios is a clear evidence for the dominant contribution from other pathways, most probably from the heterogeneous reactions.

If we assume heterogeneous chemistry to be the answer to the high  $\text{SO}_4^{2-}$  and  $\text{NO}_3^-$  concentrations, there is a problem because heterogeneous chemistry still requires oxidation by oxidizing agents, e.g., OH,  $\text{O}_3$ , etc., which were indeed significantly reduced (Sect. 6.1). Our explanation for this puzzle is that despite reduced oxidant concentrations, the aerosol volume/surface increases so much (due to elevated aerosol

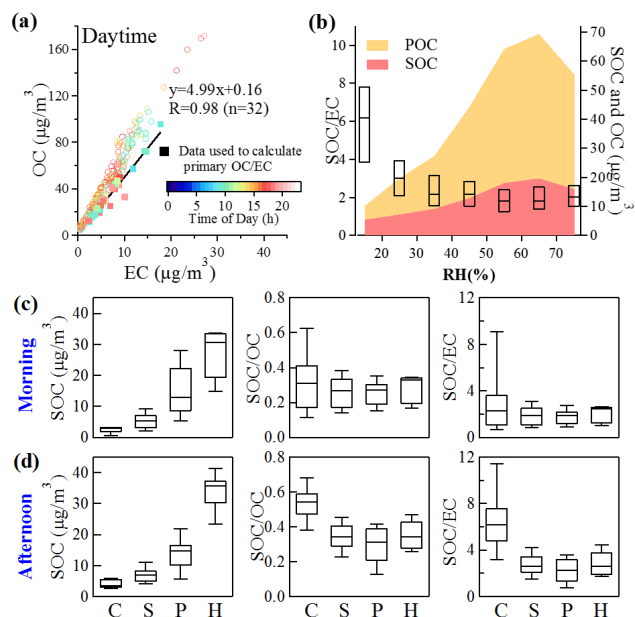


**Figure 9.** Evaluation of SOC formation. (a) Estimation of SOC with EC-tracer method. Squares indicate data used to calculate primary OC/EC, while open circles indicate other OC/EC data. (b) Change of SOC, OC and SOC/EC with RH. Data points shown in (a) and (b) referred to hourly concentrations in daytime (07:00–18:00). (c–d) Variation of SOC, SOC/OC and SOC/EC (c) in the morning (07:00~12:00) and (d) in the afternoon (13:00~18:00) with pollution level. “C”, “S”, “P”, “H” refer to “clean”, “slightly polluted”, “polluted” and “heavily polluted”, respectively. In the box-whisker plots, the boxes (b, c, d) and whiskers (c, d) indicated the 95th, 75th, 50th (median), 25th and 5th percentiles, respectively.

concentration and the accompanied high RH, Fig. 1) that it is enough to compensate its influence, and moreover, leads to a net increase in the formation of secondary aerosols.

A simplified case study could show how aerosol volume/surface increases could compensate the effect of oxidant reduction, and even lead to a net increase in the formation of secondary aerosols. Take sulfate for example: the production rate of sulfate ( $S(\text{VI})$ ) through heterogeneous reactions can be estimated by

$$dC_{S(\text{VI})}/dt \approx k[S(\text{IV})(\text{aq})] \cdot [\text{oxidants}(\text{aq})] \cdot V_{\text{aerosol}}, \quad (4)$$

in which  $C_{S(\text{VI})}$  is the sulfate concentration,  $k$  is the effective rate coefficient,  $[S(\text{IV})(\text{aq})]$  is the  $S(\text{IV})$  concentration in the aqueous phase of aerosols,  $[\text{oxidants}(\text{aq})]$  is the concentration of oxidants in the aqueous phase of aerosols, and  $V_{\text{aerosol}}$  is the volume concentration of humidified aerosol at ambient RH.

Equation (4) shows that the oxidants and  $V_{\text{aerosol}}$  are both essential for the heterogeneous reactions. From the clean to the heavily polluted case,  $\text{O}_3$  is reduced by 80%, dropping from  $>50 \mu\text{g m}^{-3}$  to  $<10 \mu\text{g m}^{-3}$  (Y. Wang et al., 2014). Based on our model simulation results,  $\text{H}_2\text{O}_2$  concentration also

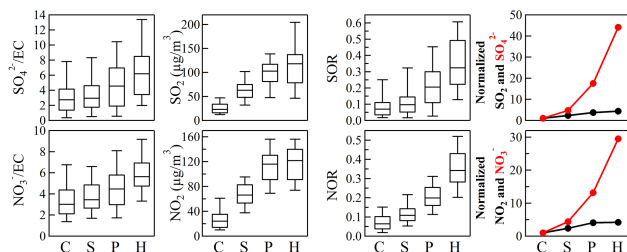


**Figure 10.** Variation of  $\text{SO}_4^{2-}/\text{EC}$ ,  $\text{NO}_3^-/\text{EC}$ ,  $\text{SO}_2$ ,  $\text{NO}_2$ , SOR and NOR with pollution level. “C”, “S”, “P”, “H” refer to “clean”, “slightly polluted”, “polluted” and “heavily polluted”, respectively. Normalized  $X$  in Column 4 refers to the average concentration of  $X$  in any pollution level, scaled by its average concentration during clean periods. In the box-whisker plots, the boxes and whiskers indicated the 95th, 75th, 50th (median), 25th and 5th percentiles, respectively.

dropped significantly from  $\sim 78$  ppbV to  $\sim 11$  ppbV. Thus we assume an upper limit of 90% reduction in  $[\text{oxidants}(\text{aq})]$ .  $V_{\text{aerosol}}$  depends on the dry aerosol concentrations  $V_{\text{dry}}$  and its hygroscopic growth factor (GF) of particle size, which is a function of RH. Assuming a constant aerosol dry density,  $V_{\text{dry}}$  is proportional to the mass concentration. From the clean case to the heavily polluted case, average  $\text{PM}_{2.5}$  mass concentration increased by 25 times, changing from  $18 \mu\text{g m}^{-3}$  to  $450 \mu\text{g m}^{-3}$  while average RH increased from dry ( $\sim 20\%$ ) to  $\sim 70\%$ . Thus we have

$$\begin{aligned} & \frac{[\text{oxidants}(\text{aq})]_{\text{HP}}}{[\text{oxidants}(\text{aq})]_{\text{Clean}}} \times \frac{(V_{\text{aerosol}})_{\text{HP}}}{(V_{\text{aerosol}})_{\text{Clean}}} \\ &= \frac{[\text{oxidants}(\text{aq})]_{\text{HP}}}{[\text{oxidants}(\text{aq})]_{\text{Clean}}} \times \frac{(V_{\text{dry}})_{\text{HP}}}{(V_{\text{dry}})_{\text{Clean}}} \times (\text{GF}_{\text{HP}/\text{Clean}})^3 \\ &\approx 0.1 \times 25 \times (1.1)^3 = 3.33, \end{aligned} \quad (5)$$

where HP and Clean indicate heavily polluted and clean periods, respectively. A GF of 1.1 was taken from previous measurements in Beijing (Meier et al., 2009).

Equation (2) shows that the increase of aerosol volume concentrations could sufficiently compensate the effect of oxidant reduction, resulting in a net increase of sulfate production.

Similarly, for  $\text{NO}_3^-$ , the influence of oxidant reduction could also be compensated by the increase of aerosol volume concentrations. There might be other oxidants associated with heterogeneous reactions, such as  $\text{O}_2$  (especially under the catalysis of mineral metals) and other oxidants existed in aerosol phase such as organic peroxides (Seinfeld et al., 2006).

In accordance with above discussions, both observation and model simulation supported the importance of heterogeneous reactions. Observed SOR and NOR showed an obvious dependence on RH (Fig. 11). Both SOR and NOR were constant under dry conditions ( $\text{RH} < 50\%$ ) (Fig. 11a,

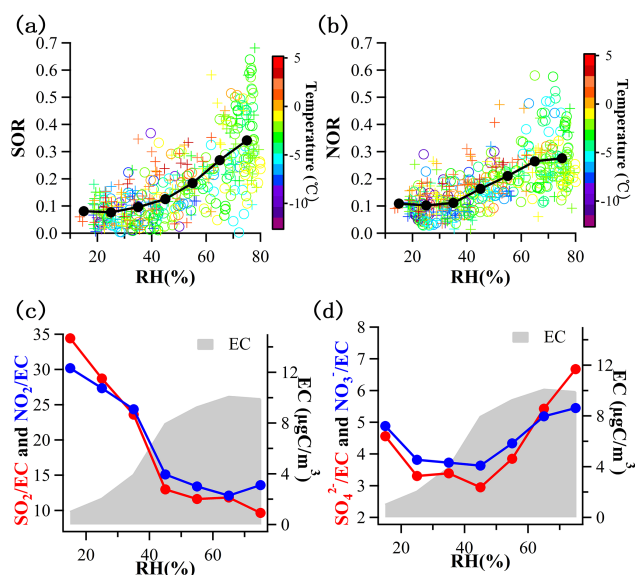


**Figure 11.** Importance of heterogeneous chemistry in sulfate and nitrate formation. (a–b) Hourly SOR and NOR plotted against RH, colored with temperature. (c–d) EC-scaled precursors ( $\text{SO}_2$  and  $\text{NO}_2$ ) and products ( $\text{SO}_4^{2-}$  and  $\text{NO}_3^-$ ) plotted against RH. EC concentrations at different RH levels were shown for reference.

b); however, started increasing when  $\text{RH} > 50\%$ , resulting in average values around 0.34 and 0.28 at  $\text{RH} 70\text{--}80\%$ , respectively. This suggests important contributions from heterogeneous reactions with abundant aerosol water under wet conditions (Sun et al., 2013a). The observed SOR value was high compared with previously reported values of 0.24 (Wang et al., 2006) and 0.29 (Zhao et al., 2013) during hazy days in Beijing. The NOR value for this study was higher than for spring hazy days in 2001–2004 (0.22; Wang et al., 2006), but significantly lower than for the hazy episode in January 2010 (0.51; Zhao et al., 2013). Our model simulation results (B. Zheng et al., 2014) also supported the importance of heterogeneous chemistry in sulfate and nitrate productions (Figure R1). With the addition of the heterogeneous reactions, the revised CMAQ showed much better performance in the polluted periods (B. Zheng et al., 2014), which demonstrated the importance of heterogeneous reaction in the production of secondary aerosols.

Concerning the SOA formation, the contribution of heterogeneous reactions might be possible, but it should be much less significant than for sulfate and nitrate. For  $\text{RH} > 50\%$ ,  $\text{SO}_4^{2-}/\text{EC}$  and  $\text{NO}_3^-/\text{EC}$  ratios rose significantly (Fig. 11d) while  $\text{SOC}/\text{EC}$  ratios remained constant (Fig. 9b). By using HOA (hydrocarbon-like organic aerosol) instead of EC, Sun et al. (2013a) found similar phenomena. Apparently, SOC doesn't have a heterogeneous formation pathway as effective as those of sulfate and nitrate.

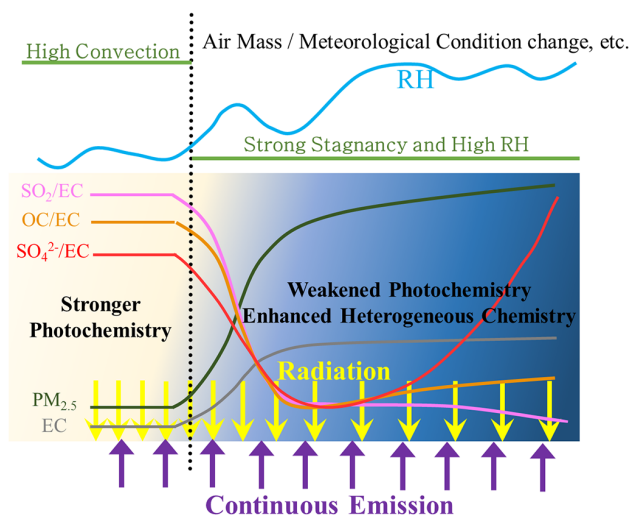


**Figure 12.** Conceptual model of atmospheric chemistry during the heavy pollution events. The dotted black line indicated the meteorology changed from a convection-favoring condition to a stagnant condition.

## 7 Conclusions

The severe haze pollution during January 2013 was not a Beijing-localized phenomenon. Rather, it was the result of local pollutants superposed on background regional pollution, which affected the whole NCP. Although pollutant emissions were high, there was no abrupt enhancement in 2013. The occurrence of the severe winter haze resulted from stable synoptic meteorological conditions over a large area of northeastern China. Surface weather maps from hazy periods were characterized by a weak high-pressure center northeast of Beijing, while the termination of a haze episode was always accompanied by the Siberian anticyclone (Xu et al., 2011; Jia et al., 2008; Liu et al., 2013). Atmospheric chemistry and physics during severe haze pollution events are illustrated in a conceptual model (Fig. 12). With the onset of stable synoptic conditions, RH rises, primary pollutants begin to accumulate and regional pollution begins to form. If the stable conditions last long enough,  $\text{PM}_{2.5}$  build-up occurs, and as a consequence, solar radiation is reduced at the ground level. This inhibits surface temperature fluctuation, making the formation of the inversed layer easier and rendering the atmosphere into a more stable condition. Meanwhile, photochemical activity is weakened under low solar radiation, and secondary aerosol formation via this pathway becomes less important. However, under high RH, heterogeneous reactions may play a more important role, especially those associated with the aerosol aqueous phase. This results in the rapid build-up of secondary aerosols, especially sulfates and nitrates, enhancing  $\text{PM}_{2.5}$  pollution. The accumulation of aerosol particles terminates with the incursion of a strong cold front, usually the Siberian anticyclone.

Our analysis also reveals that the regional transport can be a key process controlling the variations of local air pollutant concentrations. Take the sharp increases of aerosol concentrations on 11–13 January for example: Beijing pollution was temporarily flushed away by strong winds associated with the arrival of a weak cold air current; as its influence weakened, the polluted regional air mass readily reoccupied the Beijing area, resulting in an apparent rapid build-up of PM<sub>2.5</sub>. This was supported by data on the PM<sub>2.5</sub> levels around Beijing, specific humidity and PBL height, as well as surface weather maps. Our results reveal that the apparent formation rate (the rate of change in PM<sub>2.5</sub> or other air pollutants) is not only due to chemical reactions but also controlled by the regional transport along with other processes. It requires caveats to derive a real chemical production rate based on a single-site measurement. Our results also show a clear impact of regional transport on the local air pollution, suggesting the importance of regional-scale emission control measures in the local air quality management of Beijing.

**The Supplement related to this article is available online at doi:10.5194/acp-15-2969-2015-supplement.**

*Acknowledgements.* This work was supported by the National Natural Science Foundation of China (21190054, 21221004, 21107061, 41222036 and 41330635), China's National Basic Research Program (2010CB951803), China's Public Program of Ministry of Environmental Protection (201209007), and the Japan International Cooperation Agency. F. K. Duan acknowledges support from a National Excellent Doctoral Dissertation of China Award (2007B57). Y. Cheng was supported by the China Postdoctoral Science Foundation (2013T60130 and 2013M540104). D. Chang, H. Su and Y. F. Cheng were supported by the Max Planck Society (MPG) and the EU project PEGASOS (265148).

Edited by: M. Shao

## References

Blitz, M. A., Hughes, K. J., and Pilling, M. J.: Determination of the high-pressure limiting rate coefficient and the enthalpy of reaction for OH+SO<sub>2</sub>, *J. Phys. Chem. A*, 107, 1971–1978, doi:10.1021/jp026524y, 2003.

Cao, C., Jiang, W., Wang, B., Fang, J., Lang, J., Tian, G., Jiang, J., and Zhu, T. F.: Inhalable Microorganisms in Beijing's PM<sub>2.5</sub> and PM<sub>10</sub> Pollutants during a Severe Smog Event, *Environ. Sci. Technol.*, 48, 1499–1507, 2014.

Carmichael, G. R., Streets, D. G., Calori, G., Amann, M., Jacobson, M. Z., Hansen, J., and Ueda, H.: Changing trends in sulfur emissions in Asia: Implications for acid deposition, air pollution, and climate, *Environ. Sci. Technol.*, 36, 4707–4713, doi:10.1021/es011509c, 2002.

Chan, C. K. and Yao, X.: Air pollution in mega cities in China, *Atmos. Environ.*, 42, 1–42, 2008.

Chen, Y., Sheng, G., Bi, X., Feng, Y., Mai, B., and Fu, J.: Emission factors for carbonaceous particles and polycyclic aromatic hydrocarbons from residential coal combustion in China, *Environ. Sci. Technol.*, 39, 1861–1867, 2005.

Cheng, Y. F., Eichler, H., Wiedensohler, A., Heintzenberg, J., Zhang, Y. H., Hu, M., Herrmann, H., Zeng, L. M., Liu, S., Gnauk, T., Brüggemann, E., and He, L. Y.: Mixing state of elemental carbon and non-light-absorbing aerosol components derived from in situ particle optical properties at Xinken in Pearl River Delta of China, *J. Geophys. Res.*, 111, doi:10.1029/2005JD006929, 2006.

Cheng, Y. F., Heintzenberg, J., Wehner, B., Wu, Z. J., Su, H., Hu, M., and Mao, J. T.: Traffic restrictions in Beijing during the Sino-African Summit 2006: aerosol size distribution and visibility compared to long-term in situ observations, *Atmos. Chem. Phys.*, 8, 7583–7594, doi:10.5194/acp-8-7583-2008, 2008a.

Cheng, Y., Wiedensohler, A., Eichler, H., Heintzenberg, J., Tesche, M., Ansmann, A., Wendisch, M., Su, H., Althausen, D., and Herrmann, H.: Relative humidity dependence of aerosol optical properties and direct radiative forcing in the surface boundary layer at Xinken in Pearl River Delta of China: An observation based numerical study, *Atmos. Environ.*, 42, 6373–6397, 2008b.

Cheng, Y. F., Wiedensohler, A., Eichler, H., Su, H., Gnauk, T., Brüggemann, E., Herrmann, H., Heintzenberg, J., Slanina, J., Tuch, T., Hu, M., and Zhang, Y. H.: Aerosol optical properties and related chemical apportionment at Xinken in Pearl River Delta of China, *Atmos. Environ.*, 42, 6351–6372, doi:10.1016/j.atmosenv.2008.02.034, 2008c.

Cheng, Y., He, K.-b., Duan, F.-k., Zheng, M., Du, Z.-y., Ma, Y.-l., and Tan, J.-h.: Ambient organic carbon to elemental carbon ratios: Influences of the measurement methods and implications, *Atmos. Environ.*, 45, 2060–2066, doi:10.1016/j.atmosenv.2011.01.064, 2011.

Crutzen, P. J. and Birks, J. W.: Atmosphere after a nuclear war: Twilight at noon, *Ambio* (Allen Press), 11(2/3), 114–125, 1982.

Docherty, K. S., Stone, E. A., Ulbrich, I. M., DeCarlo, P. F., Snyder, D. C., Schauer, J. J., Peltier, R. E., Weber, R. J., Murphy, S. M., Seinfeld, J. H., Grover, B. D., Eatough, D. J., and Jimenez, J. L.: Apportionment of Primary and Secondary Organic Aerosols in Southern California during the 2005 Study of Organic Aerosols in Riverside (SOAR-1), *Environ. Sci. Technol.*, 42, 7655–7662, doi:10.1021/es8008166, 2008.

Duan, J., Tan, J., Yang, L., Wu, S., and Hao, J.: Concentration, sources and ozone formation potential of volatile organic compounds (VOCs) during ozone episode in Beijing, *Atmos. Res.*, 88, 25–35, doi:10.1016/j.atmosres.2007.09.004, 2008.

Hallquist, M., Wenger, J. C., Baltensperger, U., Rudich, Y., Simpson, D., Claeys, M., Dommen, J., Donahue, N. M., George, C., Goldstein, A. H., Hamilton, J. F., Herrmann, H., Hoffmann, T., Iinuma, Y., Jang, M., Jenkin, M. E., Jimenez, J. L., Kiendler-Scharr, A., Maenhaut, W., McFiggans, G., Mentel, T. F., Monod, A., Prévôt, A. S. H., Seinfeld, J. H., Surratt, J. D., Szmigielski, R., and Wildt, J.: The formation, properties and impact of secondary organic aerosol: current and emerging issues, *Atmos. Chem. Phys.*, 9, 5155–5236, doi:10.5194/acp-9-5155-2009, 2009.

He, H., Wang, Y., Ma, Q., Ma, J., Chu, B., Ji, D., Tang, G., Liu, C., Zhang, H., and Hao, J.: Mineral dust and NO<sub>x</sub> promote the

- conversion of SO<sub>2</sub> to sulfate in heavy pollution days, *Sci. Rep.*, 4, 4172, doi:10.1038/srep04172, 2014.
- He, K., Zhao, Q., Ma, Y., Duan, F., Yang, F., Shi, Z., and Chen, G.: Spatial and seasonal variability of PM<sub>2.5</sub> acidity at two Chinese megacities: insights into the formation of secondary inorganic aerosols, *Atmos. Chem. Phys.*, 12, 1377–1395, doi:10.5194/acp-12-1377-2012, 2012.
- Jia, Y., Rahn, K. A., He, K., Wen, T., and Wang, Y.: A novel technique for quantifying the regional component of urban aerosol solely from its sawtooth cycles, *J. Geophys. Res.*, 113, D21309, doi:10.1029/2008jd010389, 2008.
- Jimenez, J. L., Canagaratna, M. R., Donahue, N. M., Prevot, A. S. H., Zhang, Q., Kroll, J. H., DeCarlo, P. F., Allan, J. D., Coe, H., Ng, N. L., Aiken, A. C., Docherty, K. S., Ulbrich, I. M., Grieshop, A. P., Robinson, A. L., Duplissy, J., Smith, J. D., Wilson, K. R., Lanz, V. A., Hueglin, C., Sun, Y. L., Tian, J., Laaksonen, A., Raatikainen, T., Rautiainen, J., Vaattovaara, P., Ehn, M., Kulmala, M., Tomlinson, J. M., Collins, D. R., Cubison, M. J., Dunlea, E. J., Huffman, J. A., Onasch, T. B., Alfarra, M. R., Williams, P. I., Bower, K., Kondo, Y., Schneider, J., Drewnick, F., Borrmann, S., Weimer, S., Demerjian, K., Salcedo, D., Cottrell, L., Griffin, R., Takami, A., Miyoshi, T., Hatakeyama, S., Shimono, A., Sun, J. Y., Zhang, Y. M., Dzepina, K., Kimmel, J. R., Sueper, D., Jayne, J. T., Herndon, S. C., Trimborn, A. M., Williams, L. R., Wood, E. C., Middlebrook, A. M., Kolb, C. E., Baltensperger, U., and Worsnop, D. R.: Evolution of Organic Aerosols in the Atmosphere, *Science*, 326, 1525–1529, doi:10.1126/science.1180353, 2009.
- Kaneyasu, N., Yamamoto, S., Sato, K., Takami, A., Hayashi, M., Hara, K., Kawamoto, K., Okuda, T., and Hatakeyama, S.: Impact of long-range transport of aerosols on the PM<sub>2.5</sub> composition at a major metropolitan area in the northern Kyushu area of Japan, *Atmos. Environ.*, doi:10.1016/j.atmosenv.2014.01.029, in press, 2014.
- Khalil, M. A. K. and Rasmussen, R. A.: Tracers of wood smoke, *Atmos. Environ.*, 37, 1211–1222, doi:10.1016/s1352-2310(02)01014-2, 2003.
- Kimoto Electric Co., Ltd.: Technical Notes for Continuous Measuring Methods for Atmospheric Suspended Particulate Matters, 3rd edn., March 2012, Osaka, Japan, 2012 (in Japanese).
- Kimoto, H., Ueda, A., Tsujimoto, K., Mitani, Y., Toyazaki, Y., and Kimoto, T.: Development of a Continuous Dichotomous Aerosol Chemical Speciation Analyzer, *Clean Technology*, 23, 49–52, 2013 (in Japanese).
- Li, W. and Shao, L.: Transmission electron microscopy study of aerosol particles from the brown hazes in northern China, *J. Geophys. Res.-Atmos.*, 114, D09302, doi:10.1029/2008jd011285, 2009.
- Lim, H.-J., and Turpin, B. J.: Origins of primary and secondary organic aerosol in Atlanta: Results of time-resolved measurements during the Atlanta supersite experiment, *Environ. Sci. Technol.*, 36, 4489–4496, 2002.
- Lin, P., Hu, M., Deng, Z., Slanina, J., Han, S., Kondo, Y., Takegawa, N., Miyazaki, Y., Zhao, Y., and Sugimoto, N.: Seasonal and diurnal variations of organic carbon in PM<sub>2.5</sub> in Beijing and the estimation of secondary organic carbon, *J. Geophys. Res.*, 114, D00G11, doi:10.1029/2008jd010902, 2009.
- Liu, X. G., Li, J., Qu, Y., Han, T., Hou, L., Gu, J., Chen, C., Yang, Y., Liu, X., Yang, T., Zhang, Y., Tian, H., and Hu, M.: Formation and evolution mechanism of regional haze: a case study in the megacity Beijing, China, *Atmos. Chem. Phys.*, 13, 4501–4514, doi:10.5194/acp-13-4501-2013, 2013.
- Lu, K. D., Hofzumahaus, A., Holland, F., Bohn, B., Brauers, T., Fuchs, H., Hu, M., Häseler, R., Kita, K., Kondo, Y., Li, X., Lou, S. R., Oebel, A., Shao, M., Zeng, L. M., Wahner, A., Zhu, T., Zhang, Y. H., and Rohrer, F.: Missing OH source in a suburban environment near Beijing: observed and modelled OH and HO<sub>2</sub> concentrations in summer 2006, *Atmos. Chem. Phys.*, 13, 1057–1080, doi:10.5194/acp-13-1057-2013, 2013.
- Mauldin, R. L., Berndt, T., Sipila, M., Paasonen, P., Petaja, T., Kim, S., Kurten, T., Stratmann, F., Kerminen, V. M., and Kulmala, M.: A new atmospherically relevant oxidant of sulphur dioxide, *Nature*, 488, 193–196, doi:10.1038/nature11278, 2012.
- Meier, J., Wehner, B., Massling, A., Birmili, W., Nowak, A., Gnauk, T., Brüeggemann, E., Herrmann, H., Min, H., and Wiedensohler, A.: Hygroscopic growth of urban aerosol particles in Beijing (China) during wintertime: a comparison of three experimental methods, *Atmos. Chem. Phys.*, 9, 6865–6880, doi:10.5194/acp-9-6865-2009, 2009.
- Meng, Z. Y., Xu, X. B., Yan, P., Ding, G. A., Tang, J., Lin, W. L., Xu, X. D., and Wang, S. F.: Characteristics of trace gaseous pollutants at a regional background station in Northern China, *Atmos. Chem. Phys.*, 9, 927–936, 2009, <http://www.atmos-chem-phys.net/9/927/2009/>.
- Nel, A.: Air pollution-related illness: effects of particles, *Science*, 308, 804–806, 2005.
- Ouyang, Y.: China wakes up to the crisis of air pollution, *The Lancet Respiratory Medicine*, 1, p. 12, doi:10.1016/S2213-2600(12)70065-6, 2013.
- Peplow, M.: Beijing smog contains witches' brew of microbes, *Nature*, doi:10.1038/nature.2014.14640, 2014.
- Pöschl, U.: Atmospheric aerosols: Composition, transformation, climate and health effects, *Angew. Chem. Int. Edit.*, 44, 75200–7540, 2005.
- Plaza, J., Gomez-Moreno, F. J., Nunez, L., Pujadas, M., and Artinano, B.: Estimation of secondary organic aerosol formation from semicontinuous OC-EC measurements in a Madrid suburban area, *Atmos. Environ.*, 40, 1134–1147, doi:10.1016/j.atmosenv.2005.11.007, 2006.
- Quan, J., Tie, X., Zhang, Q., Liu, Q., Li, X., Gao, Y., and Zhao, D.: Characteristics of heavy aerosol pollution during the 2012–2013 winter in Beijing, China, *Atmos. Environ.*, 88, 83–89, doi:10.1016/j.atmosenv.2014.01.058, 2014.
- Ramanathan, V., Crutzen, P. J., Lelieveld, J., Mitra, A., Althausen, D., Anderson, J., Andreae, M., Cantrell, W., Cass, G., and Chung, C.: Indian Ocean Experiment: An integrated analysis of the climate forcing and effects of the great Indo-Asian haze, *J. Geophys. Res.*, 106, 28371–28398, 2001.
- Ramanathan, V. and Carmichael, G.: Global and regional climate changes due to black carbon, *Nat. Geosci.*, 1, 221–227, 2008.
- Saylor, R. D., Edgerton, E. S., and Hartsell, B. E.: Linear regression techniques for use in the EC tracer method of secondary organic aerosol estimation, *Atmos. Environ.*, 40, 7546–7556, doi:10.1016/j.atmosenv.2006.07.018, 2006.
- Seinfeld, J. H. and Pandis, S. N.: *Atmospheric Chemistry and Physics: from air pollution to climate change*, 2nd Edition, John Wiley and Sons, Inc., Hoboken, New Jersey, 2006.

- Stockwell, W. R. and Calvert, J. G.: The mechanism of the HO-SO<sub>2</sub> reaction, *Atmos. Environ.*, 17, 2231–2235, doi:10.1016/0004-6981(83)90220-2, 1983.
- Sun, Y., Zhuang, G., Tang, A., Wang, Y., and An, Z.: Chemical characteristics of PM<sub>2.5</sub> and PM<sub>10</sub> in haze-fog episodes in Beijing, *Environ. Sci. Technol.*, 40, 3148–3155, 2006.
- Sun, Y., Wang, Z., Fu, P., Jiang, Q., Yang, T., Li, J., and Ge, X.: The impact of relative humidity on aerosol composition and evolution processes during wintertime in Beijing, China, *Atmos. Environ.*, 77, 927–934, 2013a.
- Sun, Y., Jiang, Q., Wang, Z., Fu, P., Li, J., Yang, T., and Yin, Y.: Investigation of the Sources and Evolution Processes of Severe Haze Pollution in Beijing in January 2013, *J. Geophys. Res.*, 119, 4380–4398, 2014.
- Sun, Y. L., Wang, Z. F., Fu, P. Q., Yang, T., Jiang, Q., Dong, H. B., Li, J., and Jia, J. J.: Aerosol composition, sources and processes during wintertime in Beijing, China, *Atmos. Chem. Phys.*, 13, 4577–4592, doi:10.5194/acp-13-4577-2013, 2013b.
- Tang, G., Wang, Y., Li, X., Ji, D., Hsu, S., and Gao, X.: Spatial-temporal variations in surface ozone in Northern China as observed during 2009–2010 and possible implications for future air quality control strategies, *Atmos. Chem. Phys.*, 12, 2757–2776, doi:10.5194/acp-12-2757-2012, 2012.
- Wang, K., Zhang, Y., Nenes, A., and Fountoukis, C.: Implementation of dust emission and chemistry into the Community Multiscale Air Quality modeling system and initial application to an Asian dust storm episode, *Atmos. Chem. Phys.*, 12, 10209–10237, doi:10.5194/acp-12-10209-2012, 2012.
- Wang, L. T., Wei, Z., Yang, J., Zhang, Y., Zhang, F. F., Su, J., Meng, C. C., and Zhang, Q.: The 2013 severe haze over southern Hebei, China: model evaluation, source apportionment, and policy implications, *Atmos. Chem. Phys.*, 14, 3151–3173, doi:10.5194/acp-14-3151-2014, 2014.
- Wang, Y., Zhuang, G., Sun, Y., and An, Z.: The variation of characteristics and formation mechanisms of aerosols in dust, haze, and clear days in Beijing, *Atmos. Environ.*, 40, 6579–6591, 2006.
- Wang, Y., Yao, L., Wang, L., Liu, Z., Ji, D., Tang, G., Zhang, J., Sun, Y., Hu, B., and Xin, J.: Mechanism for the formation of the January 2013 heavy haze pollution episode over central and eastern China, *Sci. China Earth Sci.*, 57, 14–25, 2014.
- Wang, Z., Li, J., Wang, Z., Yang, W., Tang, X., Ge, B., Yan, P., Zhu, L., Chen, X., and Chen, H.: Modeling study of regional severe hazes over mid-eastern China in January 2013 and its implications on pollution prevention and control, *Sci. China Earth Sci.*, 57, 3–13, 2014.
- Wendisch, M., Hellmuth, O., Ansmann, A., Heintzenberg, J., Engelmann, R., Althausen, D., Eichler, H., Mueller, D., Hu, M., and Zhang, Y.: Radiative and dynamic effects of absorbing aerosol particles over the Pearl River Delta, China, *Atmos. Environ.*, 42, 6405–6416, 2008.
- Xing, L., Fu, T. M., Cao, J. J., Lee, S. C., Wang, G. H., Ho, K. F., Cheng, M. C., You, C. F., and Wang, T. J.: Seasonal and spatial variability of the OM/OC mass ratios and high regional correlation between oxalic acid and zinc in Chinese urban organic aerosols, *Atmos. Chem. Phys.*, 13, 4307–4318, doi:10.5194/acp-13-4307-2013, 2013.
- Xu, J., Ma, J. Z., Zhang, X. L., Xu, X. B., Xu, X. F., Lin, W. L., Wang, Y., Meng, W., and Ma, Z. Q.: Measurements of ozone and its precursors in Beijing during summertime: impact of urban plumes on ozone pollution in downwind rural areas, *Atmos. Chem. Phys.*, 11, 12241–12252, doi:10.5194/acp-11-12241-2011, 2011.
- Yang, F., Tan, J., Zhao, Q., Du, Z., He, K., Ma, Y., Duan, F., and Chen, G.: Characteristics of PM<sub>2.5</sub> speciation in representative megacities and across China, *Atmos. Chem. Phys.*, 11, 5207–5219, doi:10.5194/acp-11-5207-2011, 2011.
- Yang, K., Dickerson, R. R., Carn, S. A., Ge, C., and Wang, J.: First observations of SO<sub>2</sub> from the satellite Suomi NPP OMPS: Widespread air pollution events over China, *Geophys. Res. Lett.*, 40, 4957–4962, 2013.
- Yao, X. H., Chan, C. K., Fang, M., Cadle, S., Chan, T., Mulawa, P., He, K. B., and Ye, B. M.: The water-soluble ionic composition of PM<sub>2.5</sub> in Shanghai and Beijing, China, *Atmos. Environ.*, 36, 4223–4234, doi:10.1016/s1352-2310(02)00342-4, 2002.
- York, D., Evensen, N. M., Martinez, M. L., and Delgado, J. D.: Unified equations for the slope, intercept, and standard errors of the best straight line, *Am. J. Phys.*, 72, 367–375, doi:10.1119/1.1632486, 2004.
- Zhang, J. K., Sun, Y., Liu, Z. R., Ji, D. S., Hu, B., Liu, Q., and Wang, Y. S.: Characterization of submicron aerosols during a month of serious pollution in Beijing, 2013, *Atmos. Chem. Phys.*, 14, 2887–2903, doi:10.5194/acp-14-2887-2014, 2014.
- Zhang, Q., Streets, D. G., Carmichael, G. R., He, K., Huo, H., Kanari, A., Klimont, Z., Park, I., Reddy, S., and Fu, J.: Asian emissions in 2006 for the NASA INTEX-B mission, *Atmos. Chem. Phys.*, 9, 5131–5153, 2009, <http://www.atmos-chem-phys.net/9/5131/2009/>.
- Zhao, P. S., Zhang, X. L., Xu, X. F., and Zhao, X. J.: Long-term visibility trends and characteristics in the region of Beijing, Tianjin, and Hebei, China, *Atmos. Res.*, 101, 711–718, doi:10.1016/j.atmosres.2011.04.019, 2011.
- Zhao, X. J., Zhang, X. L., Xu, X. F., Xu, J., Meng, W., and Pu, W. W.: Seasonal and diurnal variations of ambient PM<sub>2.5</sub> concentration in urban and rural environments in Beijing, *Atmos. Environ.*, 43, 2893–2900, doi:10.1016/j.atmosenv.2009.03.009, 2009.
- Zhao, X. J., Zhao, P. S., Xu, J., Meng, W., Pu, W. W., Dong, F., He, D., and Shi, Q. F.: Analysis of a winter regional haze event and its formation mechanism in the North China Plain, *Atmos. Chem. Phys.*, 13, 5685–5696, doi:10.5194/acp-13-5685-2013, 2013.
- Zheng, B., Zhang, Q., Zhang, Y., He, K. B., Wang, K., Zheng, G. J., Duan, F. K., Ma, Y. L., and Kimoto, T.: Heterogeneous chemistry: a mechanism missing in current models to explain secondary inorganic aerosol formation during the January 2013 haze episode in North China, *Atmos. Chem. Phys.*, 15, 2031–2049, doi:10.5194/acp-15-2031-2015, 2015.
- Zheng, G., Cheng, Y., He, K., Duan, F., and Ma, Y.: A newly identified calculation discrepancy of the Sunset semi-continuous carbon analyzer, *Atmos. Meas. Tech.*, 7, 1969–1977, doi:10.5194/amt-7-1969-2014, 2014.
- Zhou, J. M., Zhang, R. J., Cao, J. J., Chow, J. C., and Watson, J. G.: Carbonaceous and Ionic Components of Atmospheric Fine Particles in Beijing and Their Impact on Atmospheric Visibility, *Aerosol Air Qual. Res.*, 12, 492–502, doi:10.4209/aaqr.2011.11.0218, 2012.